

“Nanoparticle Characterisation via 2D Classification using Single Particle Averaging”

Iain Harley¹, Anke Kaltbeitzel¹, Francesca Mazzotta¹, Kaloian Koynov¹, Sarah S. Lembke¹,
Thao P. Doan-Nguyen¹, Katharina Landfester¹, Ingo Lieberwirth^{1*}

¹ Max Planck Institute for Polymer Research, Ackermannweg 10, 55128 Mainz, Germany

E-mail: lieberw@mpip-mainz.mpg.de

Content

1	Characterisation methods.....	3
1.1	Dynamic Light Scattering.....	3
1.2	Fluorescence Correlation Spectroscopy.....	3
1.3	Static Light Scattering.....	3
1.4	Scanning Electron Microscopy.....	4
1.5	Transmission Electron Microscopy.....	4
1.6	cryo-TEM.....	4
1.7	Nanoparticle Tracking using Darkfield microscopy.....	5
2	Materials.....	5
2.1	Synthesis of polystyrene nanoparticles PS100.....	5
2.2	Synthesis of polystyrene nanoparticles PS50.....	6
2.3	Synthesis of silica nanocapsules - Si70.....	6
2.4	Synthesis of ultrasmall silica nanocapsules – Si10.....	6
2.5	Synthesis of gold nanorods – AuNR.....	7
3	Conventional size characterisation of PS100 NPs.....	8
3.1	DLS.....	8
3.2	SLS.....	9
3.3	FCS.....	10
3.4	NPT.....	11
3.5	Electron microscopy.....	11
3.6	Image Analysis.....	12

3.6.1	Image analysis using the DetectCircles Plugin for ImageJ.....	12
3.6.2	Image Analysis with the software package Ilastik.....	14
4	Conventional size characterisation of PS100 and PS50 NP mix	16
4.1	DLS of the PS50 NPs.....	16
4.2	DLS of the PS100 / PS50 particle mix.....	16
4.3	Image Analysis.....	17
4.3.1	Analysis using the DetectCircles algorithm.....	17
4.3.2	Analysis using Ilastik software package	17
5	Conventional size characterisation of silica nanocapsules Si70	18
5.1	DLS.....	18
5.2	Image Analysis.....	19
5.2.1	Analysis using the DetectCircles algorithm.....	19
5.2.2	Analysis using Ilastik software package	19
6	Conventional size characterisation of ultrasmall silica nanocapsules Si10	22
6.1	DLS.....	22
6.2	Image Analysis.....	24
6.2.1	Analysis using the DetectCircles algorithm.....	24
6.2.2	Analysis using Ilastik software package	24
7	Single Particle Averaging – 2D-CA	24
7.1	PS100	26
7.2	PS Mix	27
7.3	Large Silica NCs.....	28
7.4	Small Silica NCs.....	29
7.5	2D-CA analysis of gold nanorods.....	30
7.6	10 nm commercial Gold Beads.....	31
8	CryoSPARC Workflow	32
9	References.....	33

1 Characterisation methods

The size distribution of the PS100 nanoparticles was characterised by dynamic (DLS) and static light scattering (SLS), nanoparticle tracking (NPT), scanning electron microscopy (SEM), transmission electron microscopy (TEM), and fluorescence correlative spectroscopy (FCS).

1.1 Dynamic Light Scattering

DLS was measured on an ALV-CGS 8F SLS/DLS 5022F goniometer (equipped with eight simultaneously working ALV 7004 correlators and eight QEAPD Avalanche photodiode detectors) (ALV, Langen, Germany). A HeNe laser (632.8 nm, 25 mW output power) was utilised as a light source. 1 μ L solution of 1 wt% solid content was added to 1 mL water and filtrated (0.45 μ m). Data was recorded at room temperature.

For comparison, DLS was also measured on using a NICOMP 380 ZLS. In this device, the hydrodynamic radius is evaluated at a wave length of 660 nm under a single measurement angle of 90°, and the temperature was stabilized at 23 °C. The hydrodynamic radius was evaluated under the assumption of a single gaussian diameter distribution but also using the unique Nicomp algorithm is capable of determining multiple peaks.

1.2 Fluorescence Correlation Spectroscopy

Fluorescence correlation spectroscopy (FCS) experiments were performed using a commercial setup (Zeiss, Germany) consisting of the module ConfoCor 2 and an inverted microscope model Axiovert 200 with a Zeiss C-Apochromat 40 \times /1.2W water immersion objective. The excitation was done by the 488 nm line of an argon laser and the collected fluorescence was filtered through a LP505 long pass emission filter before reaching the detector, an avalanche photodiode that enables single-photon counting. Eight-well polystyrene-chambered coverglass (Laboratory-Tek, Nalge Nunc International) was used as a sample cell. For each solution, a series of 10 measurements with a total duration of 5 min were performed. The confocal observation volume was calibrated using a reference dye with a known diffusion coefficient i.e. Alexa Fluor 488.

1.3 Static Light Scattering

Static light scattering (SLS) measurements were performed on an ALV spectrometer consisting of a goniometer and an ALV-5004 multiple-tau full-digital correlator (320 channels) which allows measurements over an angular range from 20° to 150°. A He-Ne Laser with a wavelength

of 632.8 nm was used as light source. For temperature controlled measurements the light scattering instrument is equipped with a thermostat from Julabo.

Diluted samples were filtered through PTFE membrane filters with a pore size of 0.45 μm (LCR syringe filters). Measurements were performed at 20 °C at different angles ranging from 30° to 150°.

1.4 Scanning Electron Microscopy

The samples were mapped using a field emission microscope (LEO (Zeiss) 1530 Gemini, Oberkochen, Germany). In contrast to the low-voltage parameters commonly used for organic nanoparticles, the PS-NPs were deliberately imaged with a relatively high acceleration voltage of 1.7 to 2 kV using the Inlens-SE detector. This has the advantage that the particles can be imaged particularly well for this detector, i.e., a strong and, therefore, easy-to-process contrast is created between the substrate (Si wafer: Plano-EM#G3390) and the particles. Most micrographs were recorded at 1.953 nm pixel size with a few exceptions of 5.859 nm.

1.5 Transmission Electron Microscopy

For TEM characterisation the samples were drop casted onto a carbon coated TEM grid. Microstructural characterisation was done using a Tecnai G2 F20 (FEI) transmission electron microscope operated at an acceleration voltage of 200 kV. Micrographs were acquired using a Gatan US1000 CCD camera.

The Si100 nanocapsules were measured using a JEOL JEM-1400 (Jeol Ltd, Tokyo, Japan) electron microscope, operated at an acceleration voltage of 120 kV. Micrographs were acquired using a Gatan US1000 CCD camera.

1.6 cryo-TEM

Samples were prepared by placing a drop of particle solution on a copper grid coated with a Lacey carbon film using a Vitrobot IV (Thermo Fisher Scientific). Excess sample solution was blotted off before plunging into liquid ethane. Particles were thus embedded in a vitrified ice film. The grids were transferred using a Gatan cryo-holder (Gatan cryo holder type 626) to a Tecnai G2 F20 (FEI) TEM microscope. Images were recorded at a voltage of 200 kV using a Gatan US1000 CCD camera

1.7 Nanoparticle Tracking using Darkfield microscopy

As an alternative method, particle size distribution was evaluated by enhanced darkfield microscopy using a Cytoviva adapter connecting a Cytoviva Light Source (EXFO X-Cite0 Q) to a Zeiss AxioScope microscope. For imaging a 100x/1.25 Achromatic oil immersion objective was used. The scattered light of the nanoparticles was recorded with a Leica DFC360FX camera at a frame time of 40 Hz. Determination of the size distribution is based on the evaluation of Brownian motion. Contrary to dynamic light scattering the diffusion coefficient is not determined via the autocorrelation function of an ensemble of nanoparticles. Instead, evaluation of the diffusion constant is based on tracking of individual nanoparticles in a time series. Videos were evaluated using the ImageJ Plugin NanoTrackJ. The hydrodynamic diameter is estimated from the diffusion coefficient of individual nanoparticles using the Stokes-Einstein relation. The analysis was based on scattered light on a video sequence with 400 frames. The parameters for the NanoTrackJ plugin were set to 60 nm minimum diameter and 10 steps minimum track length. With these settings, we were able to use 1225 identified tracks for particle size analysis.

2 Materials

2.1 Synthesis of polystyrene nanoparticles PS100

A macroemulsion was prepared with a continuous phase containing Lutensol AT50 solution (600 mg) in 24 mL Milli-Pore water as surfactant and a dispersed phase containing distilled styrene (6.01 g, $5.8 \cdot 10^{-2}$ mol), hexadecane (260 mg, $1.1 \cdot 10^{-3}$ mol) as hydrophobe, Bodipy methacrylate (6.1 mg, $1.33 \cdot 10^{-5}$ mol) as fluorescent dye and 2,2'-azobis(2-methylbutyronitrile) (V59) (103 mg, $5.4 \cdot 10^{-4}$ mol) as oil soluble azo initiator.

Both phases were homogenized by mechanical stirring and the continuous phase was added slowly to the stirring dispersed phase. The macroemulsion was stirred for 1 h at the highest speed. Subsequently, the macroemulsion was ultrasonicated with a Branson Sonifier (1/2" tip, 6.5 mm diameter) for 2 min at 450 W and 90% amplitude under ice cooling to obtain a miniemulsion. The miniemulsion was directly transferred into a 50 mL flask and stirred in an oil bath at 72 °C. The polymerization was run for 21 h. The dispersion was purified by centrifugation (2 h, 13000 rpm; 4 times), the supernatant was always removed and the pellet was redispersed in Milli-pore water.

2.2 Synthesis of polystyrene nanoparticles PS50

A macroemulsion was prepared with a continuous phase containing sodiumdodecylsulfat solution (800 mg) in 24 ml Milli-Pore water as surfactant and a dispersed phase containing distilled styrene (17.69 g, $1.7 \cdot 10^{-1}$ mol), hexadecane (754 mg, $3.3 \cdot 10^{-3}$ mol) as hydrophobe, distilled Acrylic Acid (372 mg, $5.1 \cdot 10^{-3}$ mol) for introduction of carboxy-functionalities, Bodipy methacrylate (16.2 mg, $3.5 \cdot 10^{-5}$ mol) as fluorescent dye and 2,2'-azobis(2-methylbutyronitrile) (V59) (304 mg, $1.58 \cdot 10^{-3}$ mol) as oil soluble azo initiator.

Both phases were homogenized by mechanical stirring and the continuous phase was added slowly to the stirring dispersed phase. The macroemulsion was stirred for 1 h at highest speed. Subsequently, the macroemulsion was homogenized by using a microfluidizer processor LM10 under ice cooling to obtain a miniemulsion. The miniemulsion was directly transferred into a 250 mL flask and stirred in an oilbath at 72 °C. The polymerization was run for 20 h. The dispersion was purified by dialyses (1.5 h, against 16 L Milli-pore water).

2.3 Synthesis of silica nanocapsules - Si70

For the synthesis of the silica nanocapsules tetraethoxysilane (TEOS) (TCI Chemicals, Germany; > 97 %), hexadecane (TCI Chemicals, Germany; > 98 %), cyclohexane (VWR Chemicals, Germany, ≥ 99.5 %), Cetyltrimethylammonium chloride (CTMA-Cl) (Acros Organics, Belgium; 99 %) were used as received.

Silica nanocapsules were synthesized according to a previously described procedure^{1,2} by hydrolysing and condensing the alkoxysilane at the interface of a oil nanodroplet with the continuous phase in a direct miniemulsion. The dispersed phase of the miniemulsion was prepared by mixing TEOS (2.00 g; 9.60 mmol) and hexadecane (160 mg, 0.71 mmol) with cyclohexane (1.00 g, 11.88 mmol). Subsequently, CTMA-Cl (23.1 mg, 0.07 mmol) was dissolved in 30 mL MilliQ water in order to prepare a 0.77 mg/mL^{-1} aqueous solution of CTMA-Cl as the continuous phase. Both phases were combined and pre-emulsified by stirring at 500 rpm for 1 h, before sonicating the pre-emulsion with a Branson 450 W sonifier with a 1/2" tip at 70% amplitude for 180 s in pulse mode (30 s of sonication, 10 s pause) under ice cooling. The resulting miniemulsion was stirred at 1000 rpm for 20 h.

2.4 Synthesis of ultrasmall silica nanocapsules – Si10

Tetraethyl orthosilicate (98%, Acros Organics), dimethyloctadecyl[3-(trimethoxysilyl)propyl]ammonium chloride (60% in methanol, Acros Organics), (3-aminopropyl)triethoxysilane (98%, Sigma-Aldrich), cyclohexane (99.8%, Carlo Erba),

chloroform (anhydrous, Carlo Erba), cyanine 5 NHS ester (Cy5, Fisher Scientific) were used as received. Deionized water was used throughout all experiments.

Ultrasmall silica nanocapsules were synthesized following our previous work.³ Cy5-APTES was prepared by mixing 5.21 mg of cyanine 5 NHS ester with 3.64 μ L of (3-aminopropyl)triethoxysilane (APTES) and 3 g of anhydrous chloroform. The mixture was stirred overnight. 0.134 mL of cyclohexane and 2 mL of tetraethyl orthosilicate were mixed with 0.5 mL solution of Cy5-APTES 4.3 mg/mL in chloroform to form an oil phase. The oil phase was added to 30 mL of an aqueous phase containing 3.8 mg/mL dimethyloctadecyl[3-(trimethoxysilyl)propyl]ammonium chloride in water. The mixture was pre-emulsified by vigorous stirring for 30 minutes. The emulsion was then sonicated under ice-cooling in a pulse regime (3 seconds on, 3 seconds off) with 50 % amplitude using a Branson SFX 550 sonifier. The miniemulsion was stirred at 25 °C for 20 hours and then at 40 °C for 6 hours.

The synthesized dispersion contained about 11% of “large” nanocapsules (diameter > 100 nm) and 89% of ultrasmall nanocapsules (diameter < 10 nm). The large nanocapsules were removed by centrifugating the dispersion twice (10,000 rpm, 4 °C, 45 minutes).

2.5 Synthesis of gold nanorods – AuNR

For the synthesis of the gold nanorods chloroauric acid ($[\text{HAuCl}_4] \cdot 3\text{H}_2\text{O}$, Sigma Aldrich, $\geq 99.9\%$), cetyltrimethylammonium bromide (CTAB, Acros Organics, 99 %), sodium borohydride (NaBH_4 , Sigma-Aldrich, 98 %), silver nitrate (AgNO_3 , Sigma-Aldrich, $\geq 99\%$) and hydrogen peroxide solution (H_2O_2 , Sigma-Aldrich 34.5 – 26.5 %) were used as received.

Gold nanorods were synthesised by adding 40.2 μ L of a 25 mM aqueous HAuCl_4 solution to 4 mL of 0.1 M CTAB solution. Subsequently, 24 μ L of a freshly prepared 0.1 M NaBH_4 solution were added to the solution while stirring at 625 rpm for 1 min. The obtained seed solution was aged at 28°C for 2 h while shaking at 200 rpm.

The growth solution was prepared by adding 80 μ L of an aqueous 0.1 M AgNO_3 solution and 1.648 mL of the 25 mM HAuCl_4 solution to 80 mL of 0.1 M CTAB solution while stirring at 250 rpm. While stirring at 375 rpm for 1 min 43.6 μ L of 34.5% H_2O_2 solution were added to the growth solution before adding 240 μ L of the seed solution and stirring at 400 rpm for 30 s. The resulting solution was aged at 28 °C for 1.5 h. The gold nanorods were centrifuges at 14000 rpm for 20 min at 28 °C two times in order to wash them with deionized water. Afterwards the gold nanorods were resuspended in deionized water.

3 Conventional size characterisation of PS100 NPs

In order to obtain a good overview of the actual size distribution of the PS100 model system, we have carried out a thorough characterization using various measurement methods. This allows us to conclusively evaluate the values obtained with the 2D-CA and to validate the quality of our new image analysis. The entire extract of these measurements can be found in Table 1.

3.1 DLS

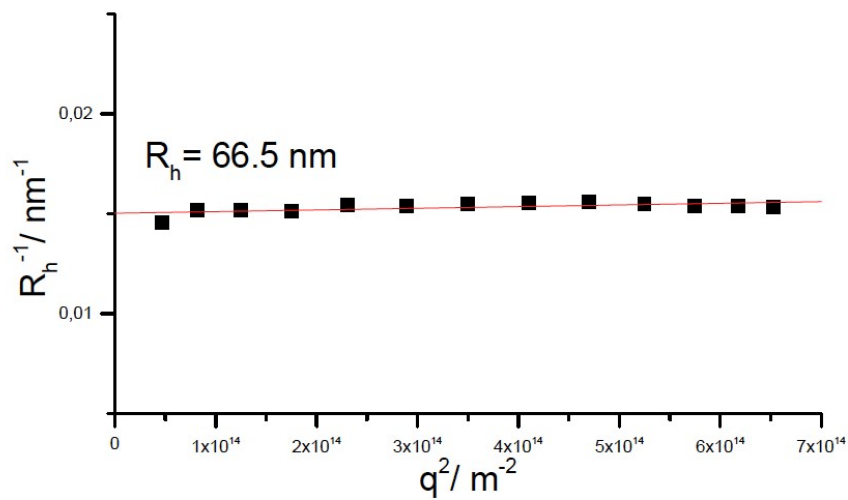
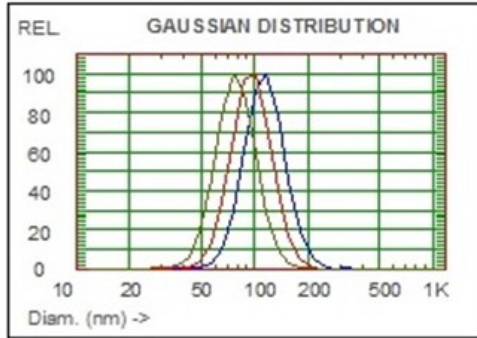


Figure S 1 - Evaluation of the intensity averaged mean diameter of PS100 by DLS.

GAUSSIAN/NICOMP DISTRIBUTION Analysis (Solid Particle)

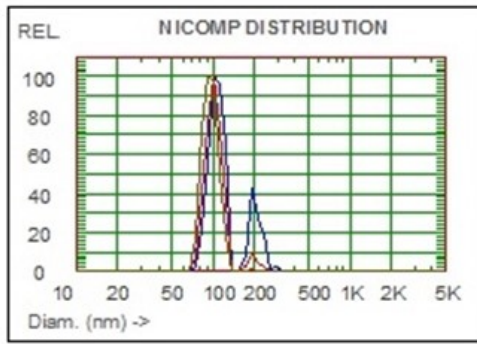
Fit Error	= 2.93	Residual	= 0.00
Chi Squared	= 1.64	Baseline Adj.	= 0.10 %
Run Time	= 0 Hr 5 Min 5 Sec	Wavelength	= 660.0 nm
Count Rate	= 306 KHz	Temperature	= 23 deg C
Channel #1	= 400.0 K	Viscosity	= 1.000 cp
Channel Width	= 17.0 uSec	Index of Ref.	= 1.331



Intensity Weighting:
 Mean Diameter = 117.2 nm
 Std Deviation = 29.6 nm (25.30 %)

Volume Weighting:
 Mean Diameter = 99.0 nm
 Std Deviation = 25.0 nm (25.30 %)

Number Weighting:
 Mean Diameter = 80.9 nm
 Std Deviation = 20.5 nm (25.30 %)



Intensity Weighting:

	Peak 1	Peak 2	Peak 3
Mean Diam.(nm)	106.1	204.9	---
Percent (%)	69.87	30.13	---

Volume Weighting:

	Peak 1	Peak 2	Peak 3
Mean Diam.(nm)	101.5	201.6	---
Percent (%)	91.54	8.46	---

Number Weighting:

	Peak 1	Peak 2	Peak 3
Mean Diam.(nm)	96.3	196.3	---
Percent (%)	98.66	1.34	---

Intensity Wt: — Volume Wt: — Number Wt: —

Figure S 2 - Evaluation of number and intensity weighted mean diameters assuming a Gaussian distribution and using the Nicomp algorithm.

3.2 SLS

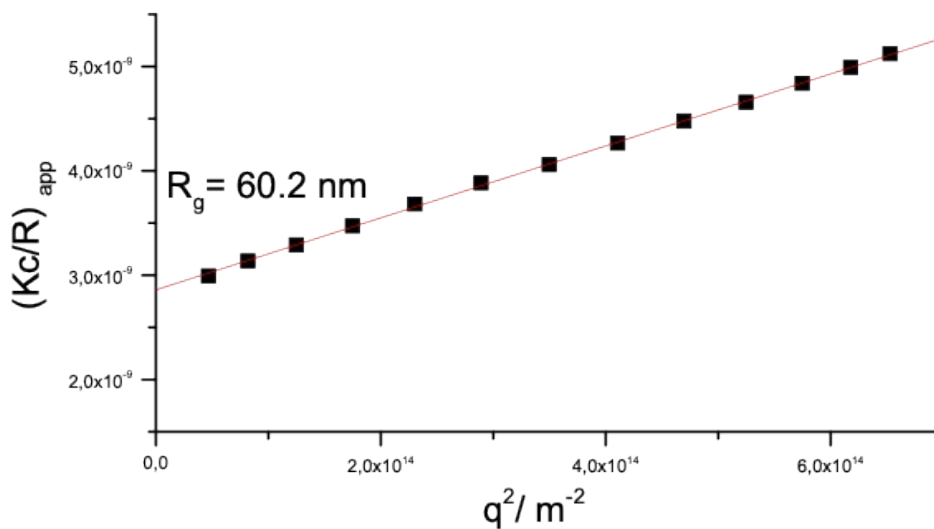


Figure S 3 – Evaluation of the intensity averaged mean diameter of PS100 by SLS. The relationship between R_g and R for spherical particles $R = \sqrt{5/3} * R_g$, a factor ~ 1.29 resulting in 155 nm as an estimate for the diameter of the particle.

3.3 FCS

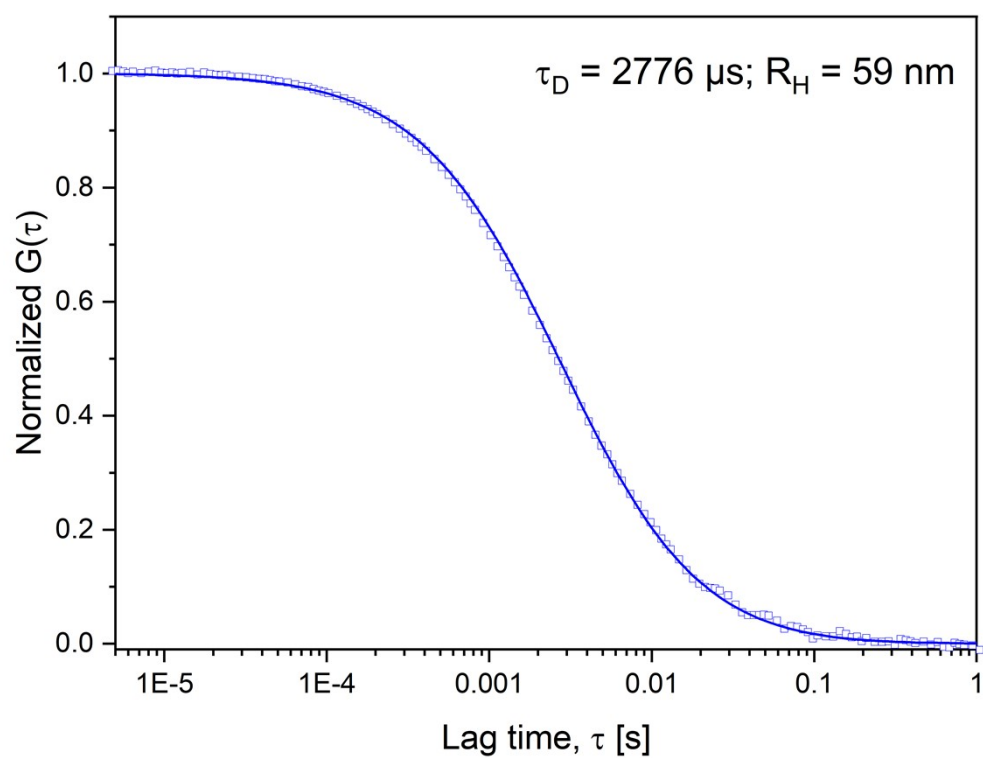


Figure S 4 – Normalised FCS autocorrelation curve of PS100 (symbols) and the corresponding fit with one-component 3D diffusion model (line) yielding the diffusion time τ_D and the hydrodynamic radius R_h of the particles.

3.4 NPT

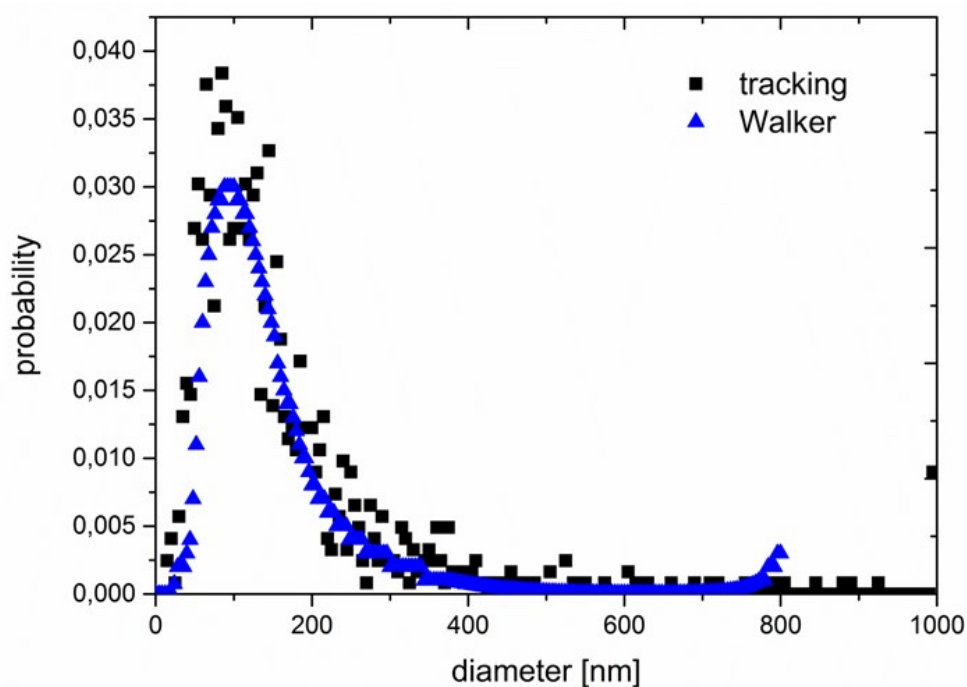


Figure S 5 - particle size distribution as evaluated by darkfield microscopy using NanoTrackJ plugin „Tracking“ mode and assuming a Walker distribution („Walker “)

3.5 Electron microscopy

The PS100 NP model system was imaged using SEM, TEM and cryo-TEM. Representative micrographs are shown in Figure S 6. These images are used for the determination of the size distribution via different image analysis methods. SEM and TEM imaging shows that the polystyrene NPs tended to cluster, likely due to the drying process. Neck-like structures connect these clusters, which could impact particle size measurement. In contrast, the TEM images show NPs that are not connected to each other. From this one can clearly conclude that the clustering of the NPs must be a drying artifact.

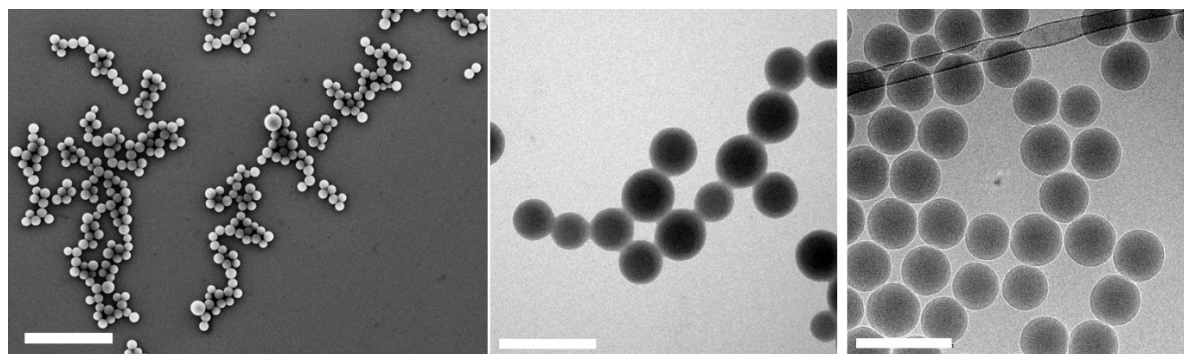


Figure S 6 – EM micrographs of the PS100 NPs showing a typical SEM (left), TEM (middle) and cryo-TEM (right) micrograph. Scale bars are 1 μm for the SEM and 200 nm for the TEM and cryo-TEM micrographs.

3.6 Image Analysis

3.6.1 Image analysis using the DetectCircles Plugin for ImageJ

The DetectCircles algorithm is able to detect circular objects based on a Hugh-Transform of the image. Here, it was used as a plugin for ImageJ, a software package dedicated to image analysis. As can be seen in Figure S 7, the NP detection efficiency is high. In total, 92 micrographs have been analysed, resulting in 11347 detected NPs. However, the amount of false positive objects (marked in blue in Figure S 7) is remarkably high. What's more, these false positives have to be sorted out manually, which involves an enormous effort. This effect becomes more dominant, the smaller the circular objects in the image, e.g. with decreasing NP diameter given in image pixels. This can be clearly seen when comparing the SEM Figure S 7 and the cryo-TEM image analysis results Figure S 8. Here, due to the higher magnification, the NPs naturally appear larger and therefore also have a larger diameter measured in pixels. Although this reduces the rate of false positives detected, the field of view is correspondingly smaller, which means that the number of NPs per image is correspondingly low.

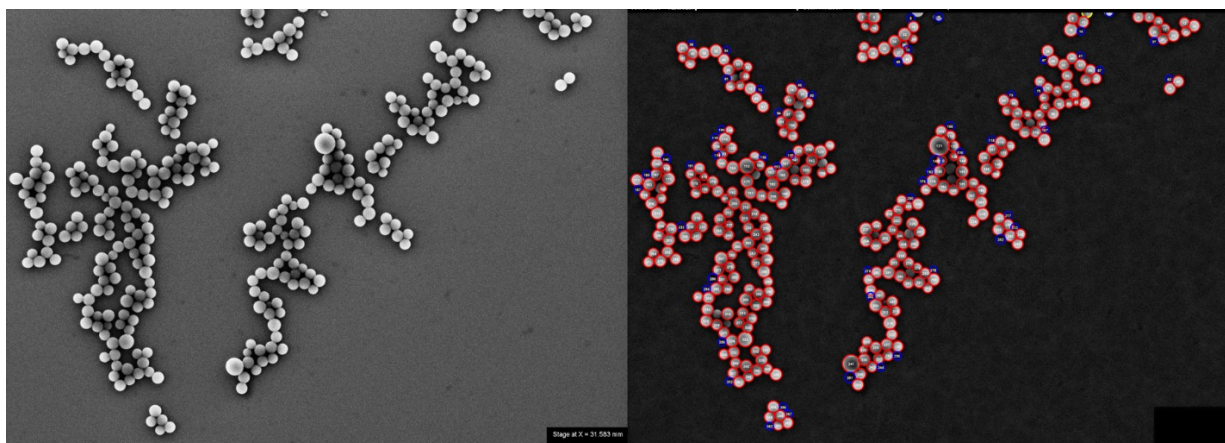


Figure S 7 -Example of SEM evaluation, top: original SEM image, lower: detection of NPs by DetectCircles after background subtraction. Red circles are correctly identified circles, blue circles are false detections. The latter were manually unselected.

Figure S 8 shows an example of the diameter evaluation of Cryo-TEM micrographs using the DetectCircles Plugin from ImageJ. Choosing appropriate scores, the circles are detected with high accuracy. All images were inspected for incorrect assignments. In some cases mismatching of circles occurred, these circles were manually untoggled in the PlugIn and thus excluded from evaluation. In total, 79 micrographs have been analysed resulting in 2986 detected NPs

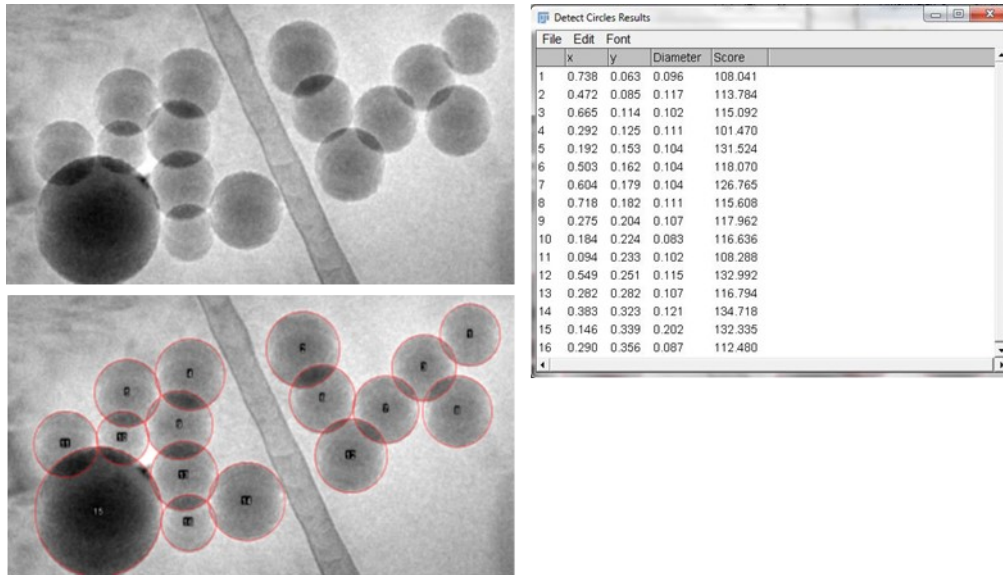


Figure S 8 - Evaluation of nanoparticle diameters from a cryo-TEM dataset using ImageJ Plugin DetectCircles

Both measurements, i.e. SEM and cryo-TEM, show quite good agreement with average diameters of 109 nm and 104 nm, respectively (Figure S 9, left). The results based on the SEM images show only a small skew towards larger values compared to the cryo-TEM measurements. A manual evaluation based on 200 measured NPs from TEM images yields an average diameter of 110 nm (Figure S 9, right). This minor discrepancy between those measurements may be attributed to factors such as binning during data analysis, the sharpness of particle edges influenced by over- or under-focus conditions, and parameters used in circle detection algorithms.

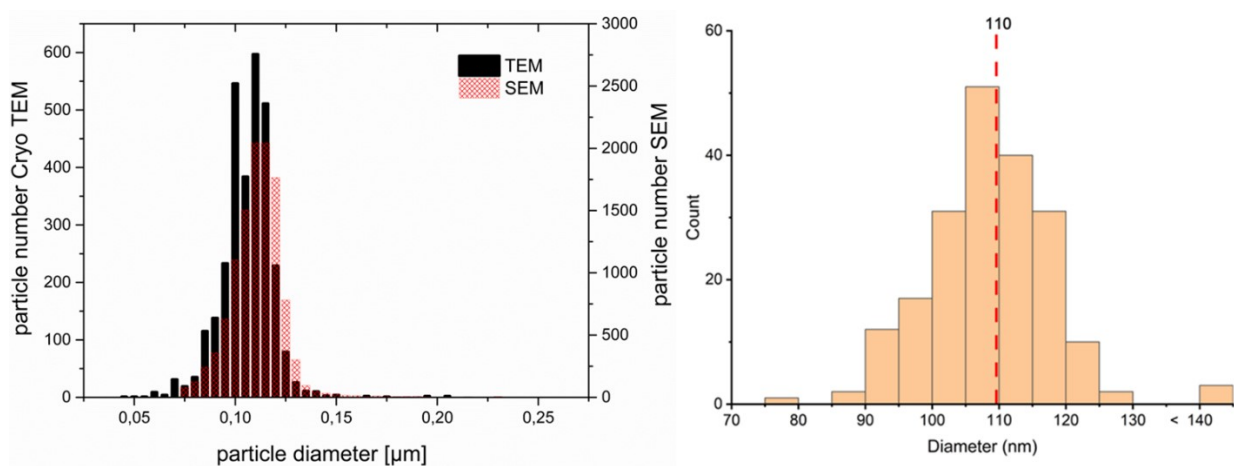


Figure S 9 –size distribution of PS100: as measured by Cryo-TEM (left axis) and SEM (right axis) using the DetectCircles algorithm (left) and a manual measurement of 200 NPs from TEM micrographs (right).

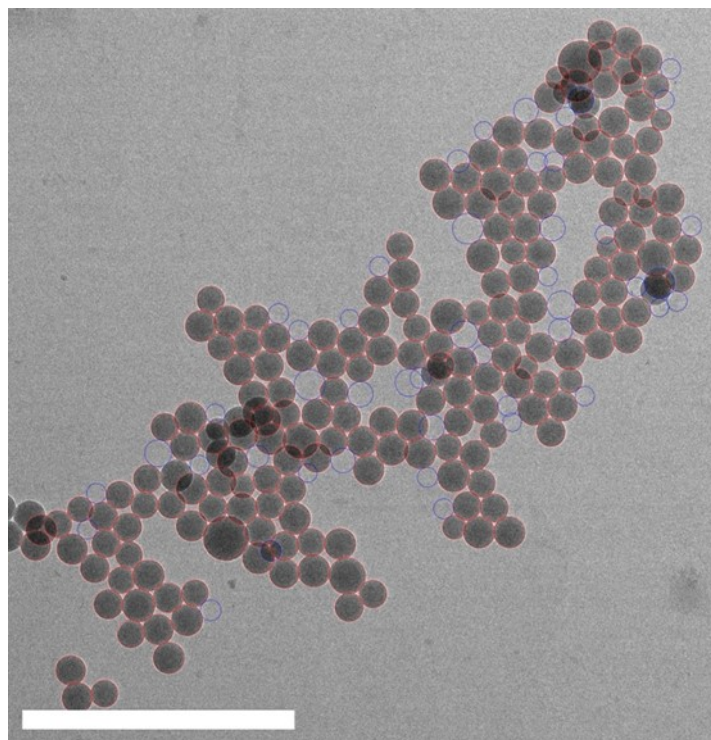


Figure S 10 - Detect Circles on PS100 NPs. Scale bar 1 μ m. Red Circles are correct picks, and blue are incorrect picks. The process and method for determining optimal detection parameters were as follows: Raw micrograph \rightarrow Convert to 8bit \rightarrow Bin by 2 \rightarrow Auto contrast. Optimal conditions – Min diameter = 70 nm max diameter = 150 nm, Min score = 121. For an initial test, this produced a total of 230 particles with an accuracy of 83 %.

3.6.2 Image Analysis with the software package Ilastik

Image analysis for particle sizing using the Ilastik software package is a two-stage classification process. For this purpose, a representative image is selected from the data set. First, the pixels in this image are divided into two classes - background and particles - by manual marking. Only a few pixels are annotated, and then the entire image is classified using statistical methods. Here it may be necessary to optimise the quality of the pixel classification by repeated annotation. The image is then segmented into object and background pixels by manually setting a threshold value. The probability of the class to which the individual pixels belong is used in this process.

Subsequently, a further classification takes place at the object level. The (geometric) objects created by the thresholding are subjected to a second supervised classification. Here, the objects/particles are again divided into two classes - those that are useful and those that are unusable for a size measurement. The latter can, for example, be particles that overlap or those for which the pixel classification has not identified the entire particle. Both are recognisable in a form that deviates from a spherical geometry. The object classification is trained on this and should then separate measurable from unmeasurable objects. In the final step, the objects

identified as measurable particles are measured geometrically; the area of the particles in the image is of particular interest here for the particle size distribution. The circle-equivalent diameter of each positively identified particle can then be easily calculated from this. However, many more geometric features can be extracted for each of the identified particles, e.g. the Feret diameters, circularity, etc. Once, the system is trained, a batch processing of the complete dataset of micrographs can be processed. However, one has to keep in mind that this workflow, especially the batch-processed micrographs, can be very susceptible to producing false positives (and true negatives) if the imaging conditions fluctuate, e.g. the contrast and brightness levels vary over the input micrographs. This is especially the case for TEM datasets, where the sample thickness – and thus the image contrast and brightness - tends to vary locally.

Moreover, Figure S11 shows another problem with this pixel-based approach. As soon as the NPs are in contact with each other, an unambiguous identification and separation of individual NPs fails.

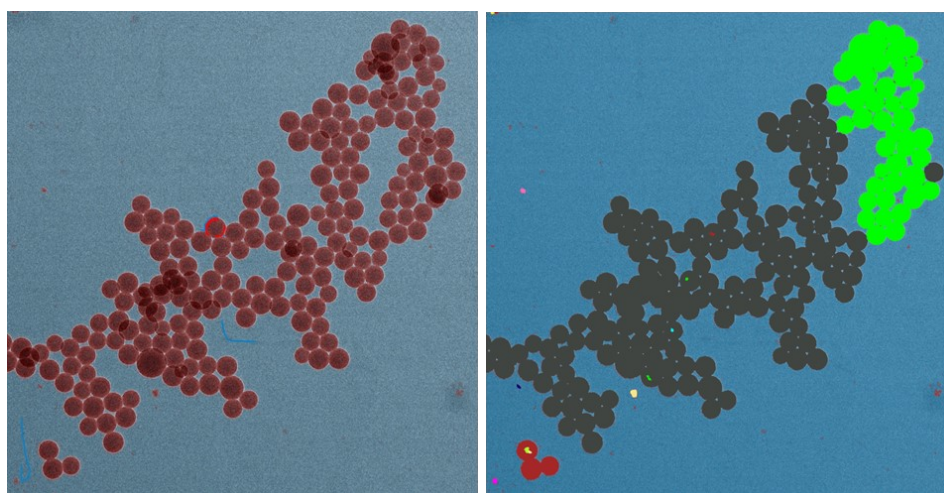


Figure S11 – Left: Pixel Classification of TEM micrograph of PS100 after only 1 refinement round. The discrimination between background and object pixels is successful. Right: The thresholding analysis, however, fails to identify individual NPs because they attach and overlap. Accordingly, only large clusters of many NPs are identified as individual objects.

4 Conventional size characterisation of PS100 and PS50 NP mix

4.1 DLS of the PS50 NPs

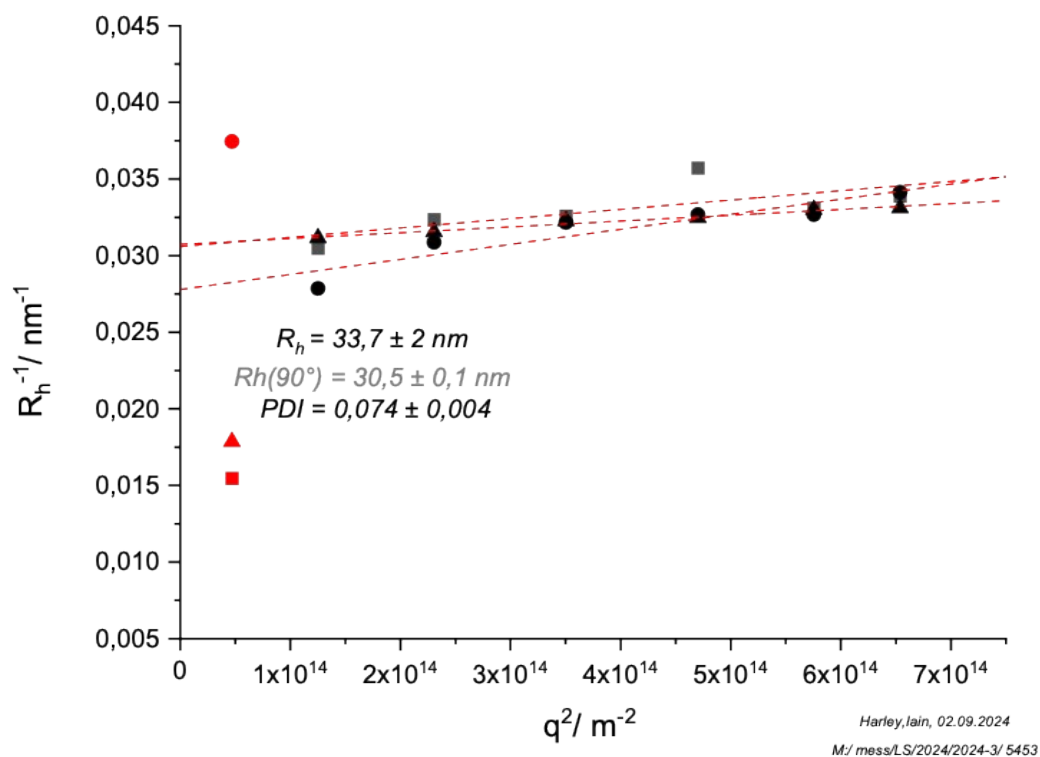


Figure S 12 – DLS of PS50 polystyrene NPs yielding a hydrodynamic diameter of 67 nm.

4.2 DLS of the PS100 / PS50 particle mix

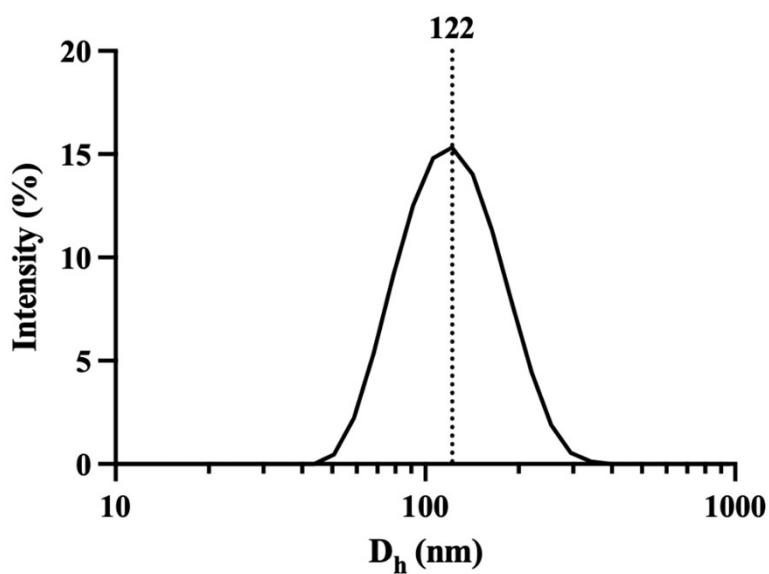


Figure S 13 – DLS of the PS100 / PS50 mix with 122 nm diameter z-average. Although both particle populations have a rather narrow size distribution, the mixed ensemble of particles is not resolved by DLS. Here, only one population with a slightly lower R_g than for the PS100 pure system is observed.

4.3 Image Analysis

4.3.1 Analysis using the DetectCircles algorithm

The DetectCircles algorithm is quite effective when the particle size distribution is very narrow, as shown in Fig S10. With a bimodal distribution, however, an extremely large number of false positive objects are detected, as can be seen in Fig. S14.

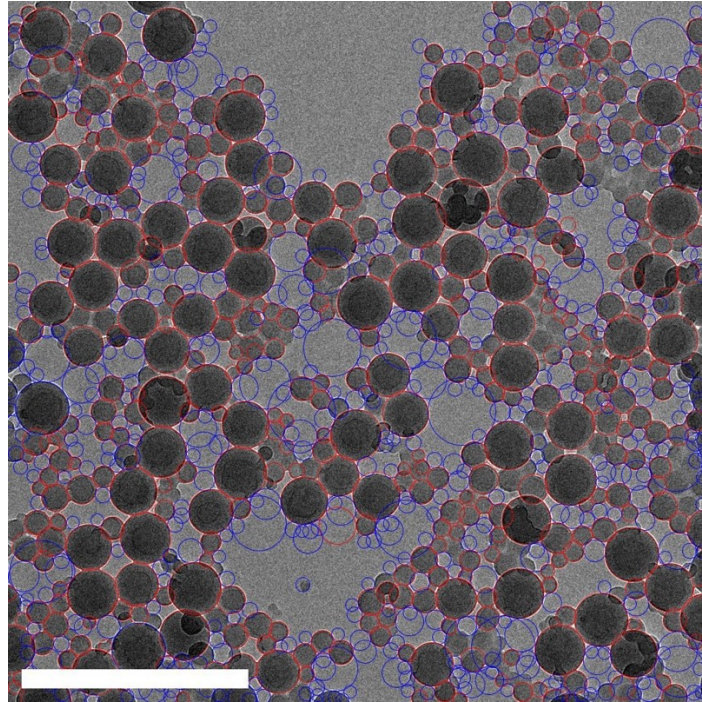


Figure S 14 - Detect Circles on PS Mix. Scale bar 500nm. Red Circles are correct picks, and blue is incorrect picks. The process and method for determining optimal detection parameters were as follows: Raw micrograph → Convert to 8bit → Bin by 2 → Auto contrast. Optimal conditions – Min diameter = 30 nm max diameter = 150 m, Min score = 40. For an initial test, this produced a total of 898 particles with an accuracy of 44%.

4.3.2 Analysis using Ilastik software package

As can be seen in Figure S 15, the pixel classification works well on this kind of micrographs. However, pixel based separation of individual particles is problematic. Thresholding can not separate overlapping particles. Hence, no analysis can be performed using Ilastik.

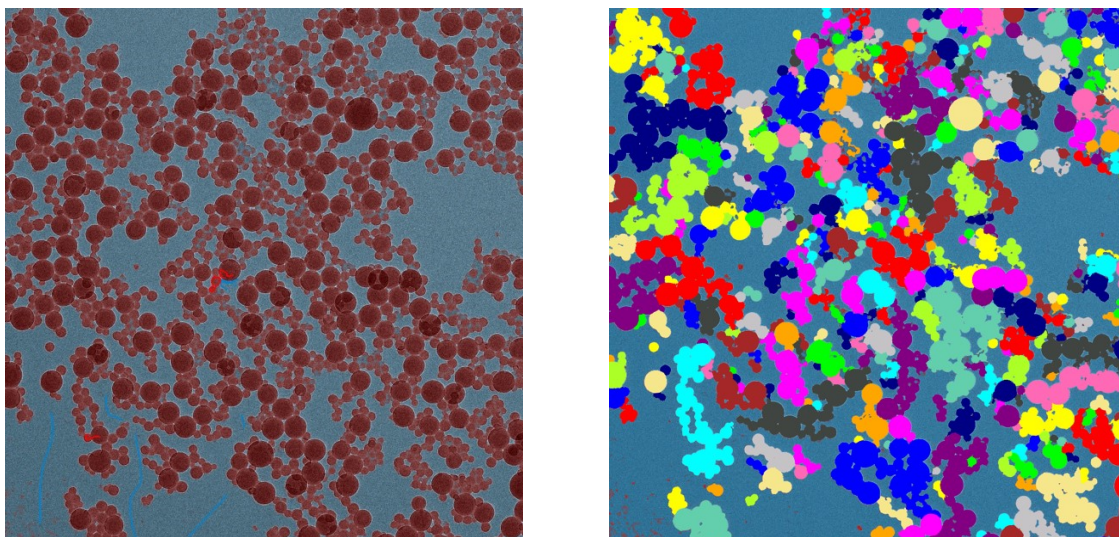


Figure S 15 – Left - Pixel Classification after one refinement round. The labels indicate the pixels used for training. Right – Thresholding analysis failed to discriminate individual particles because the TEM micrographs display a clustering of the NPs.

5 Conventional size characterisation of silica nanocapsules Si70

5.1 DLS

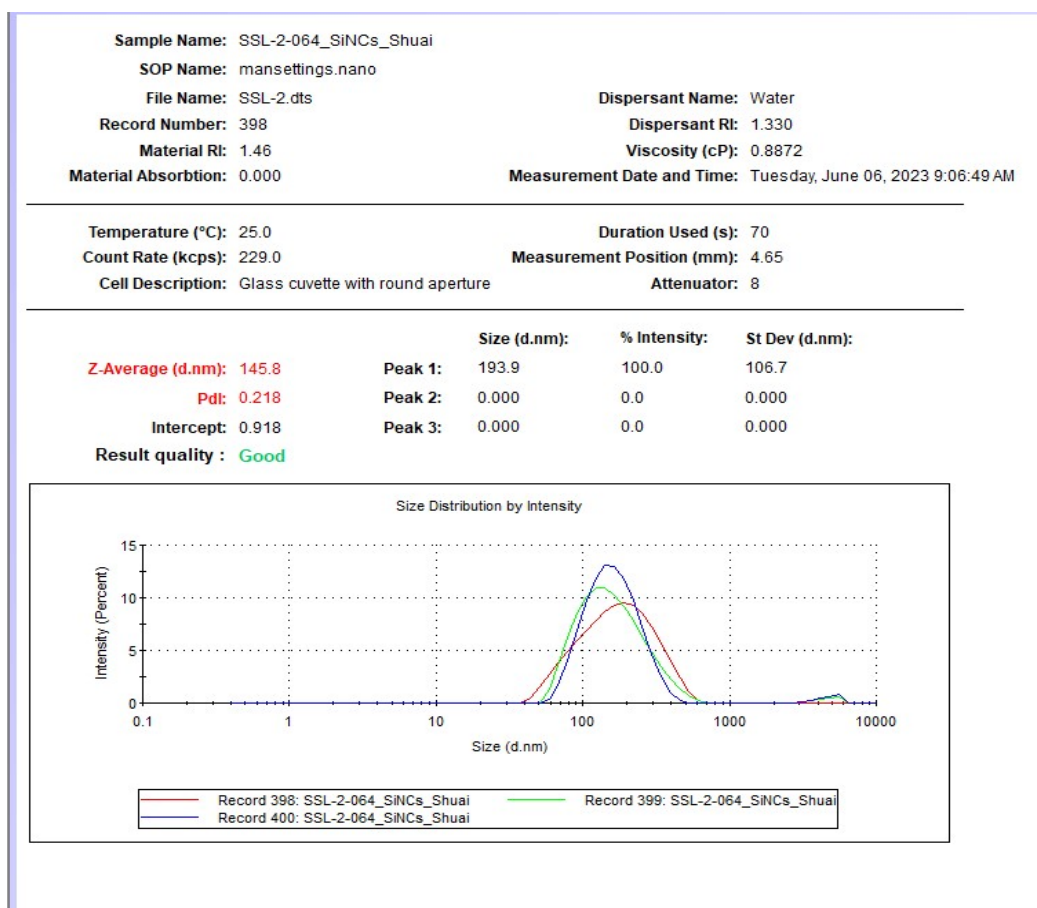


Figure S 16 - DLS of Si70 silica NCs

5.2 Image Analysis

5.2.1 Analysis using the DetectCircles algorithm

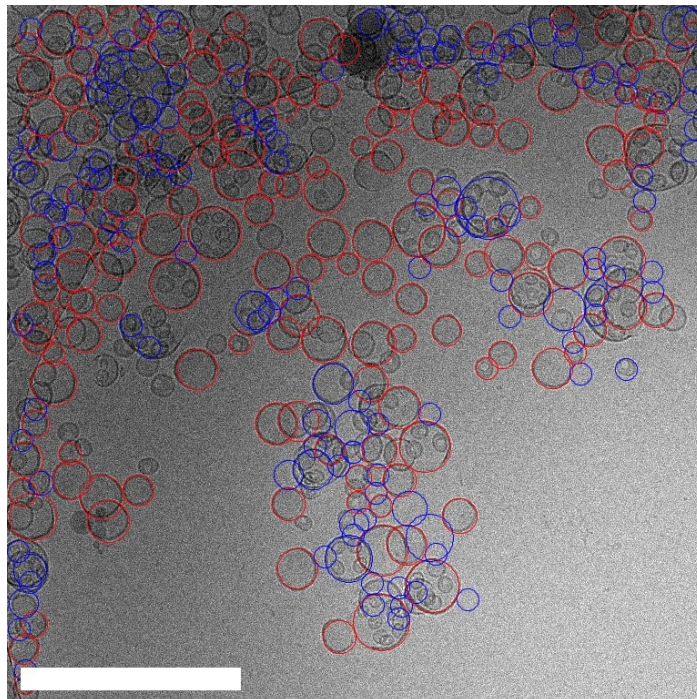


Figure S 17 -Detect Circles on Si70 silica NCs. Scale bar 500 nm. Red Circles are correct picks, and blue is incorrect picks. The process and method for determining optimal detection parameters were as follows: Raw micrograph → Convert to 8bit → Bin by 2 → Auto contrast. Optimal conditions – Min diameter = 30 nm max diameter = 150 nm, Min score = 50. For an initial test, this produced a total of 295 particles with an accuracy of 52 %

5.2.2 Analysis using Ilastik software package

Using pixel classification to identify entire capsule-like particles in Ilastik is ineffective. It's better to focus on identifying only the particle shells, leaving the core undetected. Object identification and classification are not suitable here. Instead, we trained the pixel classification specifically for the shell pixels, resulting in better detection precision.

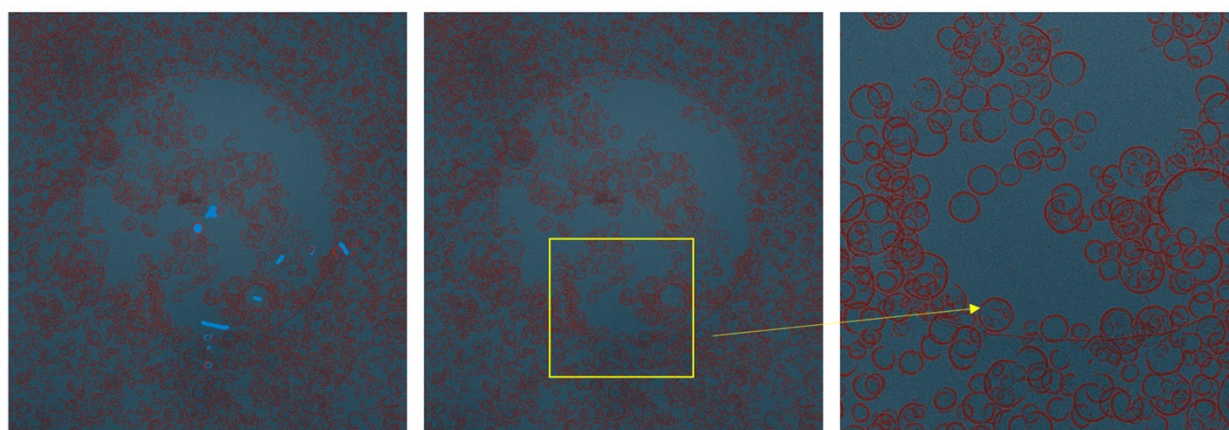
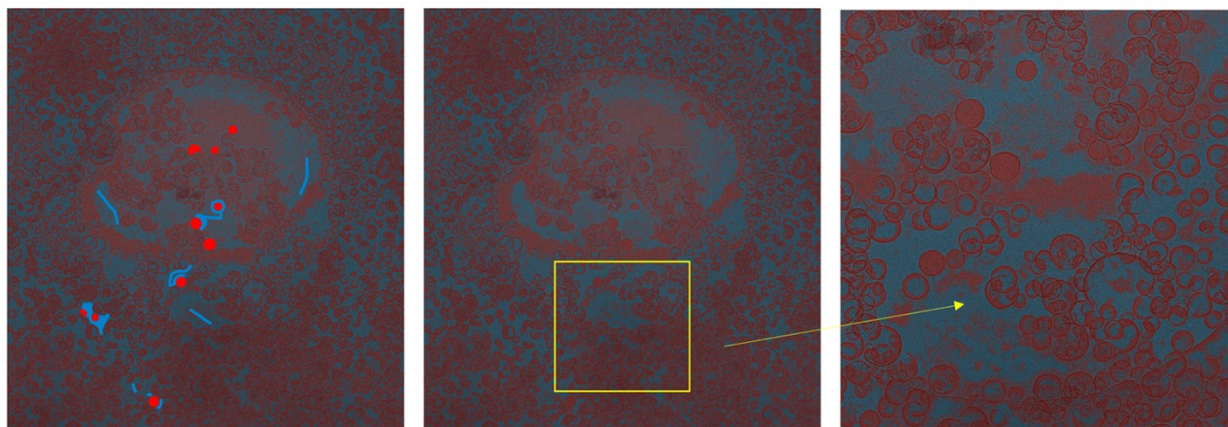


Figure S 18 - 3 rounds of rectification for the pixel classification. The labels show the areas used for training.

Figure S 19 - 1 round of rectification for the pixel classification. The labels show the areas used for training (left). Ilastik yields much better results when pixel classification is trained to find the particle shell instead of the full particle.

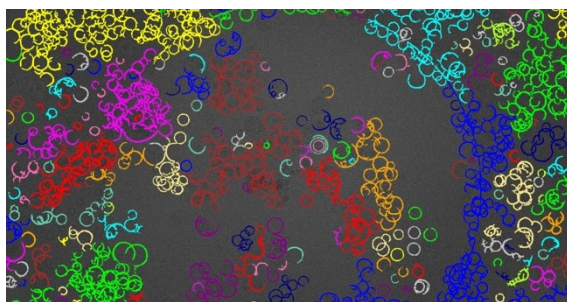


Figure S 20 - Using a threshold of 0.5 for the probability of a pixel belonging to the „red“ pixel class. Due to the high portion of overlapping particles in the initial micrograph, thresholding give a high amount of unseparable particles.



After training (pixel and object classification) we ran a batch processing with all 49 micrographs.

A total of 2081 particles was identified and their convex hull area was measured. This gives an average of 42 positive objects per micrograph. The number of false positives is not known. Average particle diameter (from convex hull area): 70 nm Standard deviation: 9 nm. For capsule-like particles, an identification of the full particle using the pixel classification step in Ilastik does not work well. Preferably, only the shell of the particles is identified; the core area remains undetected. Object identification and classification make no sense here. Instead, we trained the pixel classification only for the pixels showing the shell of the particle, which yields better results in terms of detection precision.

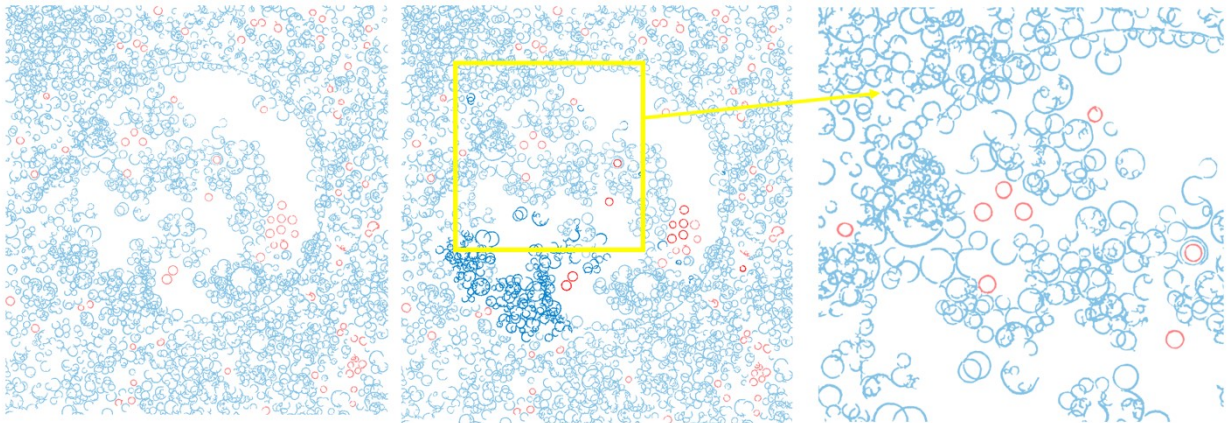


Figure S 21 - The identified objects were classified by training the software to tag spherical, separated circles only (red).

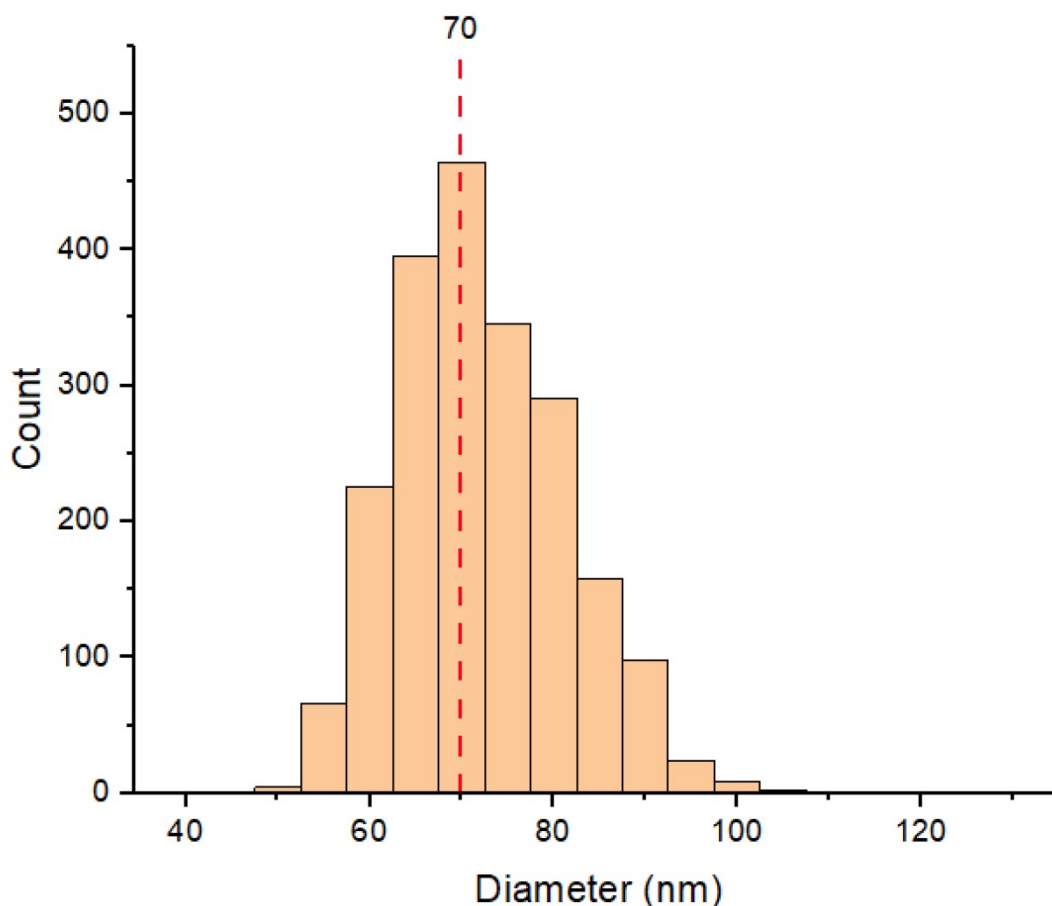


Figure S 22 - Distribution of Si70 NCs as measured by Ilastic

6 Conventional size characterisation of ultrasmall silica nanocapsules Si10

6.1 DLS

The Si10 NCs show a strong tendency to aggregate, which can be seen by DLS in Figure S 23. Here, the mean hydrodynamic diameter is 294 nm, which is an order of magnitude larger than the actual NC diameter as seen e.g. by TEM. However, if the NC is stabilized, for example by functionalization with polyethylene glycol (PEG), a significant reduction in the measured diameter is observed in the DLS, as the agglomeration is noticeably reduced here. However, a certain proportion of agglomerates can still be observed, which can be clearly seen in the measured hydrodynamic diameter (Figure S 24). Here, two DLS measurements are shown with different filtrations of the sample dispersion prior to the measurement. Filtration with a 200 nm filter results in a significant smaller R_h than a filtration with a 5 μm filter. This result indicates, that despite steric stabilization of the NCs with a PEG shell, a noticeable agglomeration is present.

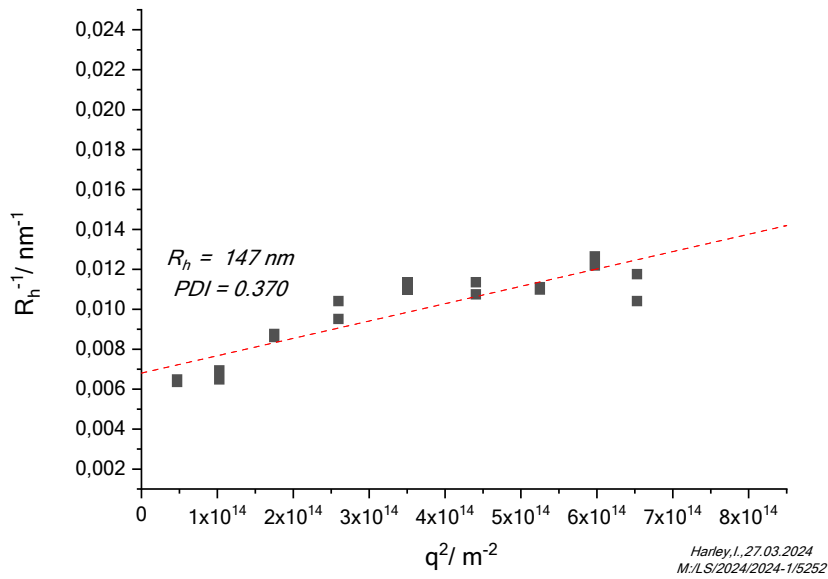


Figure S 23 – DLS of Si10 ultrasmall silica NCs with no PEG functionalisation. The measured diameter is significantly larger than expected from the TEM micrographs (Fig 6 a).

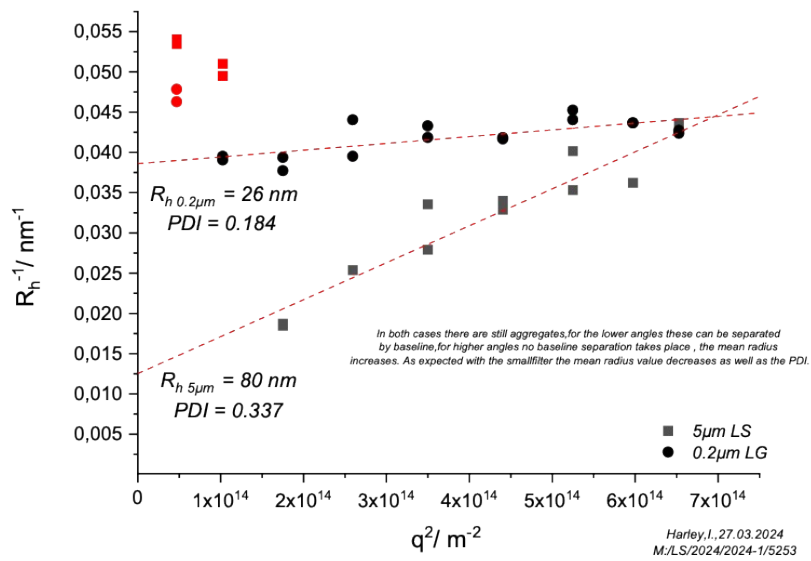


Figure S 24 - DLS of Si10 NCs with PEG functionalisation. Compared to the non-functionalized NCs, the steric stabilization yields a smaller R_h . However, filtration with a 200 nm filter yields a significantly smaller value than a filtration with a 5 µm filter. This indicates, that there are still large agglomerates in the sample dispersion, which lead to a skewing of the DLS measurement results.

6.2 Image Analysis

6.2.1 Analysis using the DetectCircles algorithm

The process and method for determining optimal deflection parameters were as follows: Raw micrograph → Convert to 8bit → Bin by 2 → Auto contrast. No conditions were found to correctly identify the small nanocapsules.

6.2.2 Analysis using Ilastik software package

For the ultra-small silica NC, the pixel classification works well on this kind of micrographs. However, pixel-based separation of individual particles is problematic and as a result, thresholding cannot separate overlapping particles. Hence, no analysis can be performed using Ilastik.

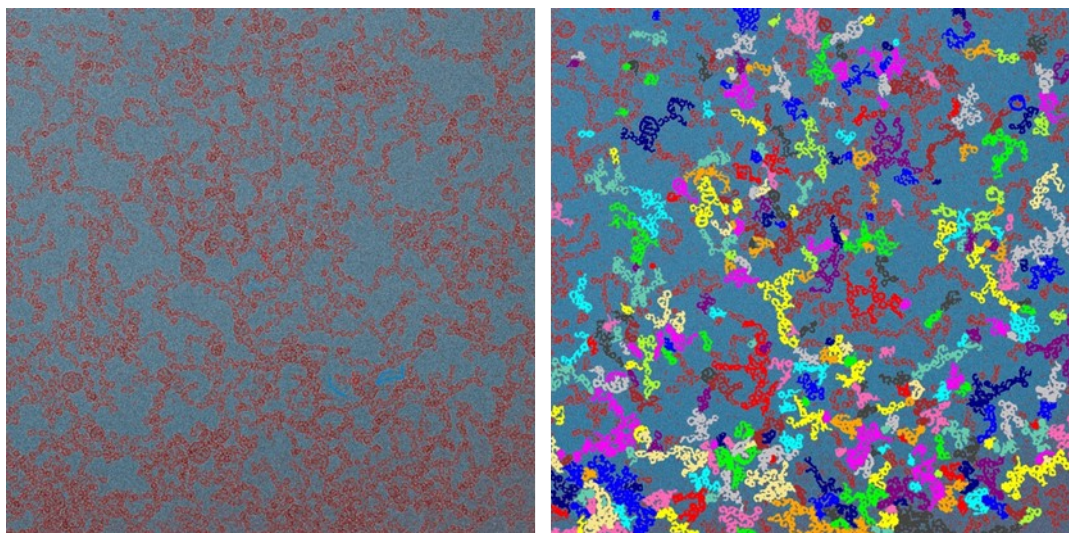


Figure S 25 – Image analysis using Ilastik pixel-and-object classification software. The pixel classification works well and the Si10 particles are efficiently discriminated from the background (left). The clustering of the Si10 NCs, however, cannot be resolved and no individual objects / NPs can be detected. Instead, large, coherent agglomerates are identified as individual particles (right).

7 Single Particle Averaging – 2D-CA

In 2D classification, we currently have no influence on the division of the particles into the different classes due to the underlying algorithm and therefore also not on the distance between the individual classes in terms of the diameter of the particles. This means, that the average diameter of each class is more or less arbitrary. As a result, the distance between the diameters of the individual classes is not uniform, as one would expect from a standard histogram display.

Rather, the 2D-CA results in a non-equidistant representation of the diameter populations, which is visually unintelligible without further processing. Figure S 26 shows the pure measurement results of the 2D-CA analysis of all investigated NP systems in the form of a diagram that plots the particle population against the average diameter of each 2D class.

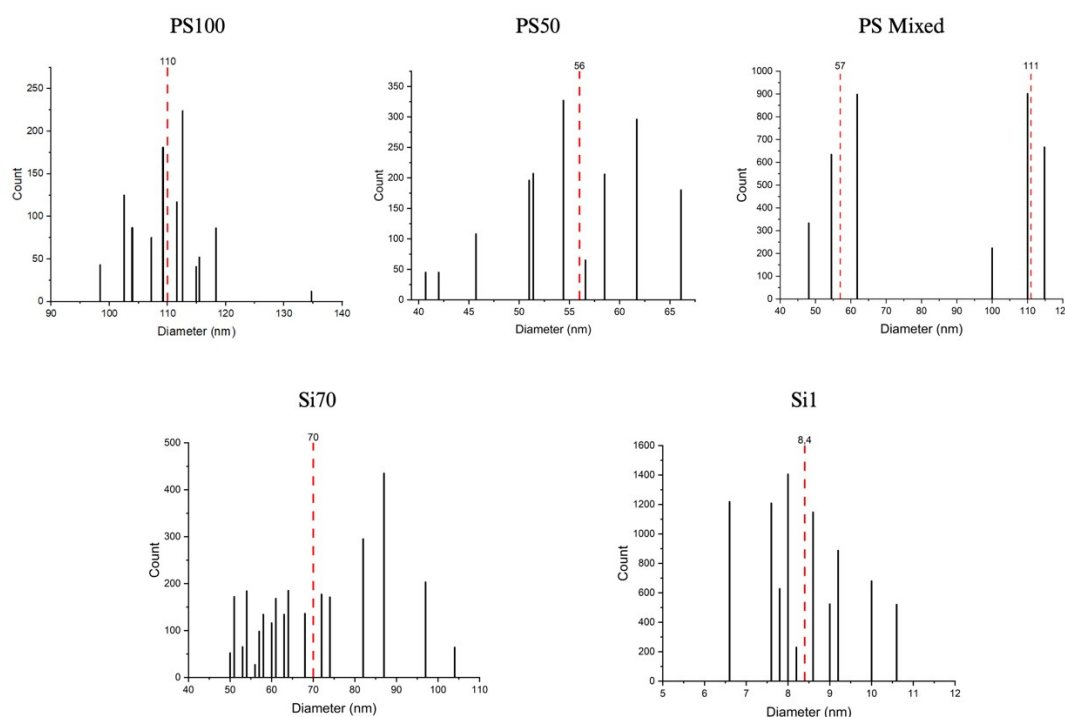


Figure S 26 - Raw (unbinned) 2D-CA results from 2D class average measurements for all measured NP systems,

In order to obtain a better representation of the 2D-CA measurements, the non-equidistant raw data must therefore be binned to generate an equidistant histogram representation. For the measurement of PS100 NPs, for example, it can be seen that there are two classes at about 115 nm in Figure S 26.

Due to the 2D-CA method providing 2D classes with non-equidistant sizes, the raw measurements were binned together to provide a better visualisation of the distribution. Such as in PS100, two classes around 115 nm are binned together, as demonstrated in Figure S 27. In order to generate a familiar size distribution histogram from the 2D-CA data, an equidistant binning is superimposed on the data, as shown in Figure S 27. In each binning, the populations of the classes falling into the corresponding binning are consolidated. Thus, we finally achieve an equidistant representation of the particle size distribution.

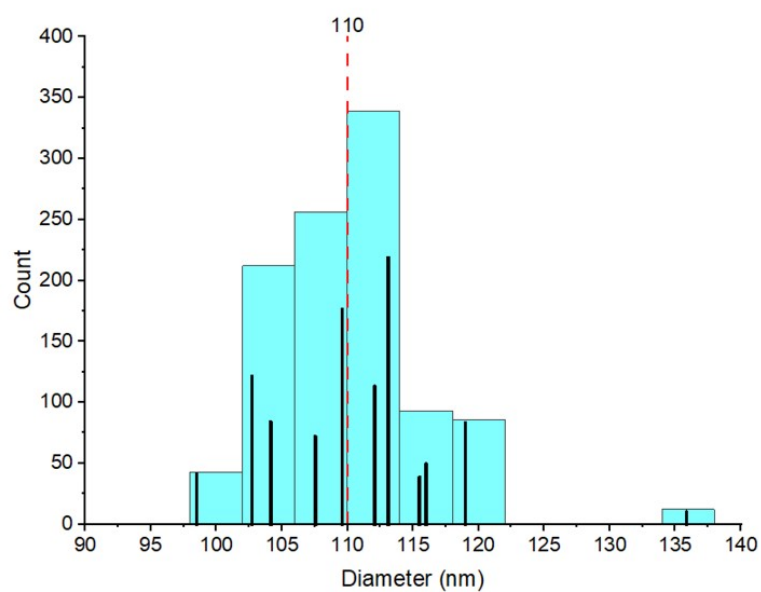


Figure S 27 – 2D-CA analysis of PS100 showing raw values and binned values, demonstrating the approach to overcome the non-equidistant binning from the 2D classification yielding a commonly known particle size distribution histogram.

7.1 PS100

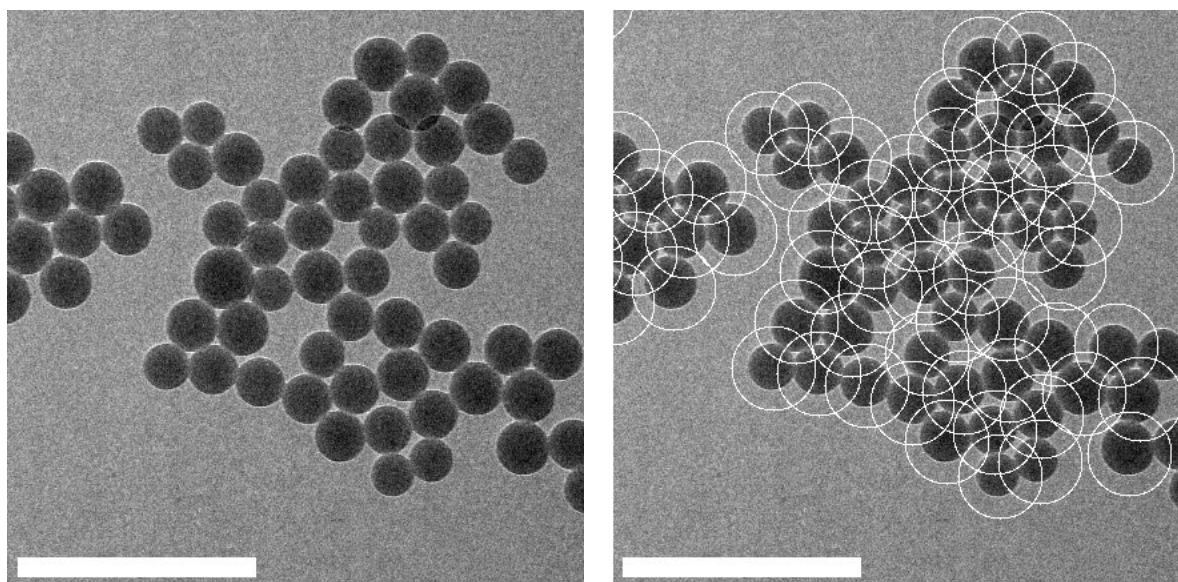


Figure S 28 - Left; raw micrograph of polystyrene particles. Right; particles selected via automated picking. Scale bar 500nm

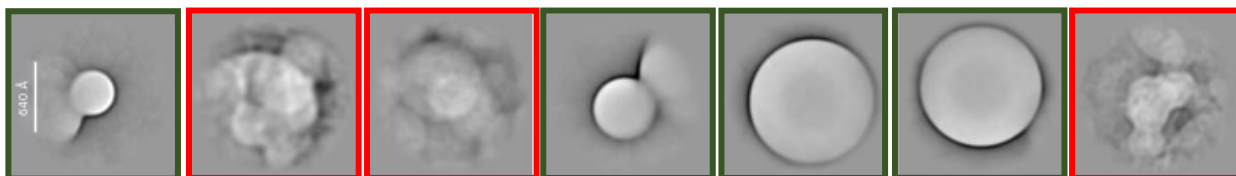


Figure S 29 – PS100 example classes from the first round after automated picking. Green boxes represent selected classes to use in further classifications; red boxes indicate classes and particles to be removed.

7.2 PS Mix

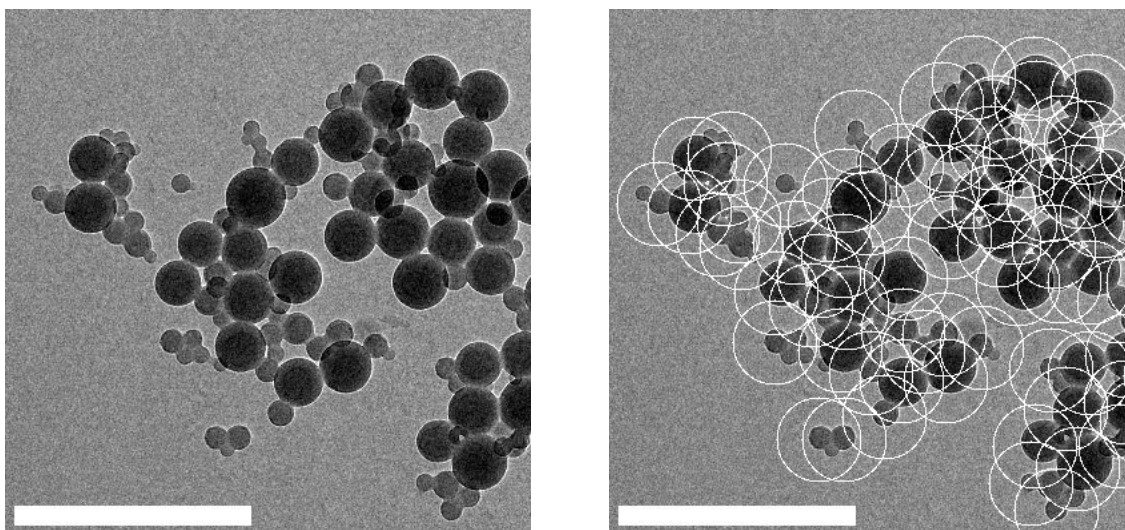


Figure S 30 - Left; raw micrograph of mixed size polystyrene particles. Right; particles selected via automated picking. Scale bar 500nm

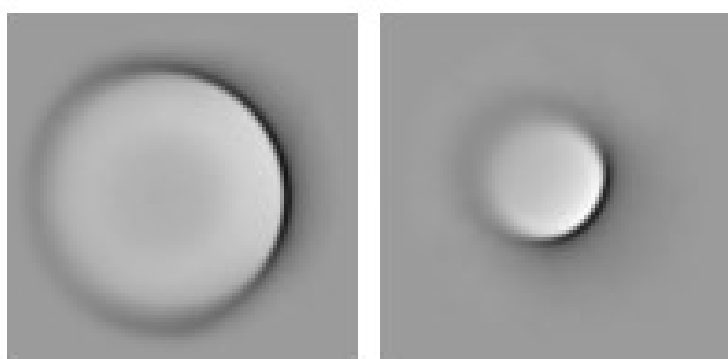


Figure S 31 - PS Mix: All particles forced into 2 classes.

7.3 Large Silica NCs

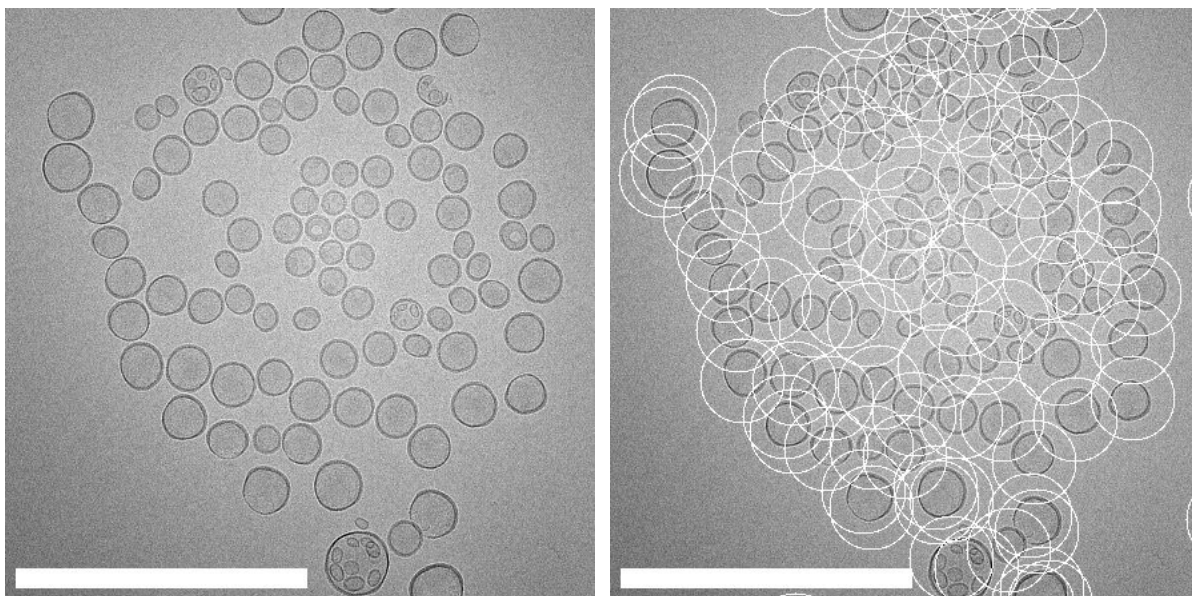


Figure S 32 - Left; raw micrograph of large silica nanocapsules. Right; particles selected via automated picking. Scale bar 500 nm.

7.4 Small Silica NCs

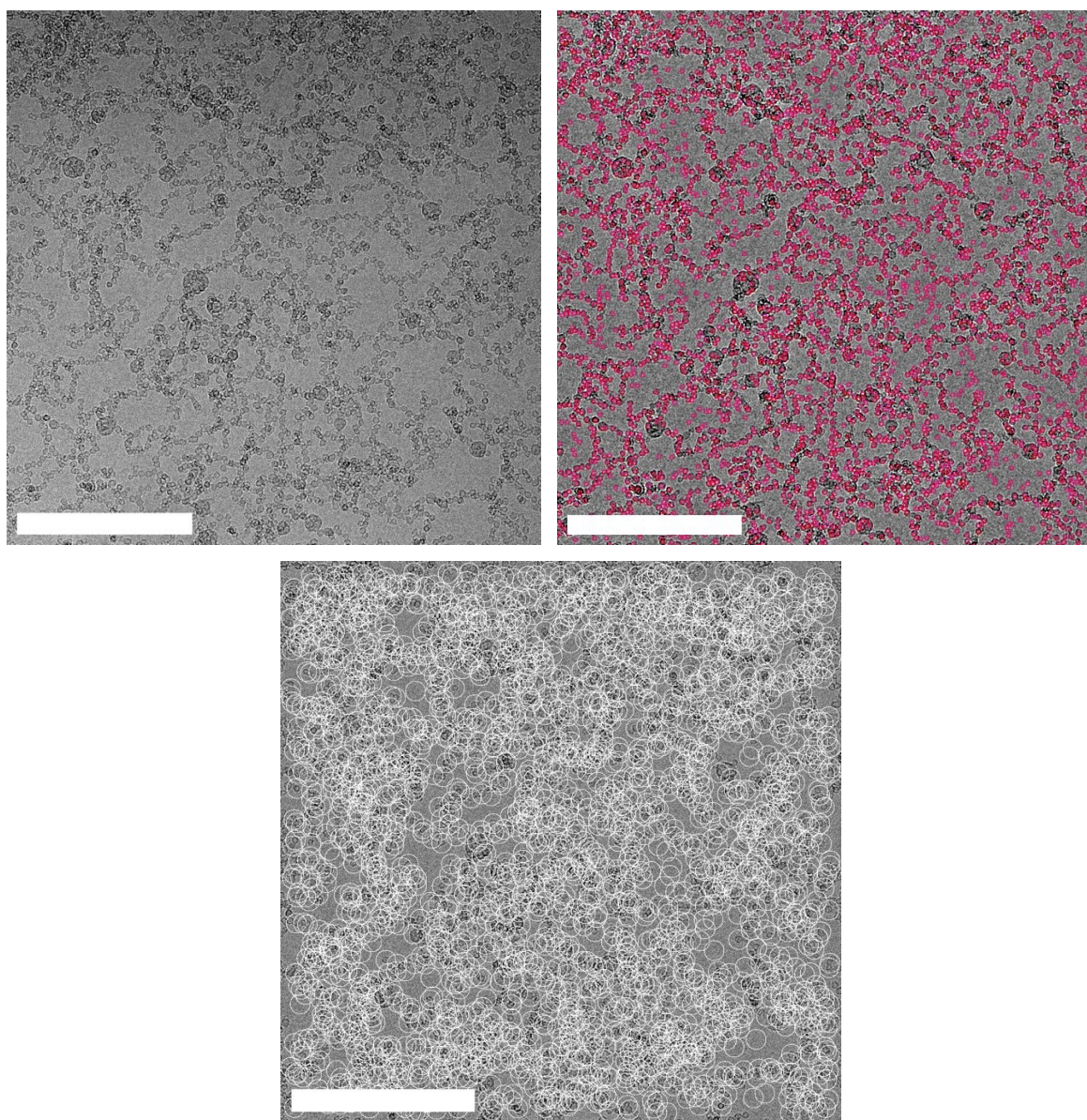


Figure S 33 - Si10 raw micrograph and subsequent picked particles using the cryoSPARC particle picking algorithm. Scale bar 500 nm.

7.5 2D-CA analysis of gold nanorods

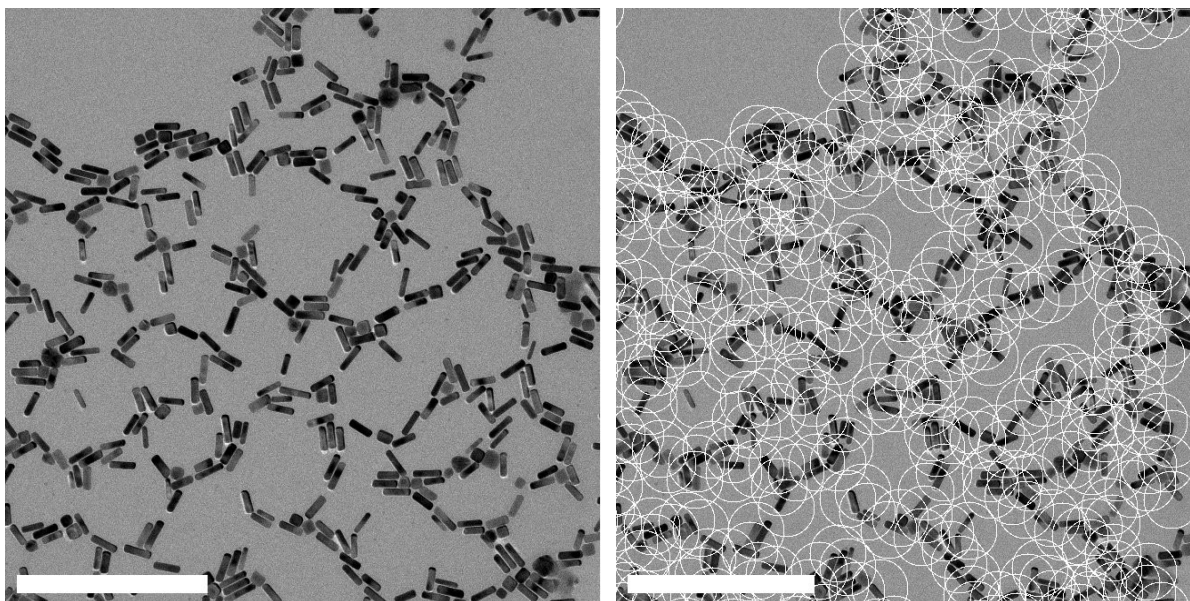


Figure S 34 - Left; raw micrograph of gold nanorods. Right; particles selected via automated picking. Scale bar 300 nm.

Additional Thresholding tests of AuNRs

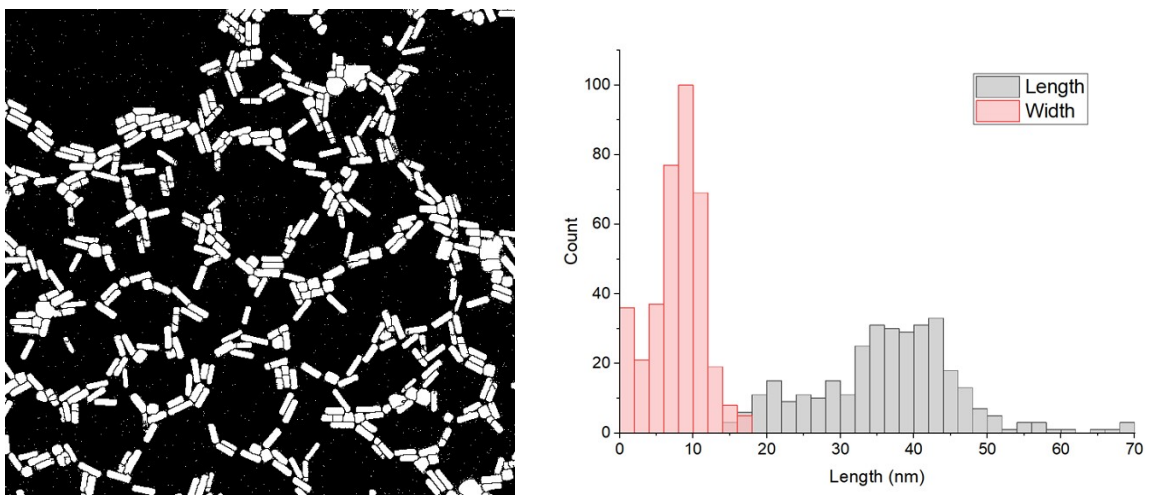


Figure S 35 – Left; threshold of gold nanorods in fiji. Right; Histogram of thresholding results with length.

7.6 10 nm commercial Gold Beads

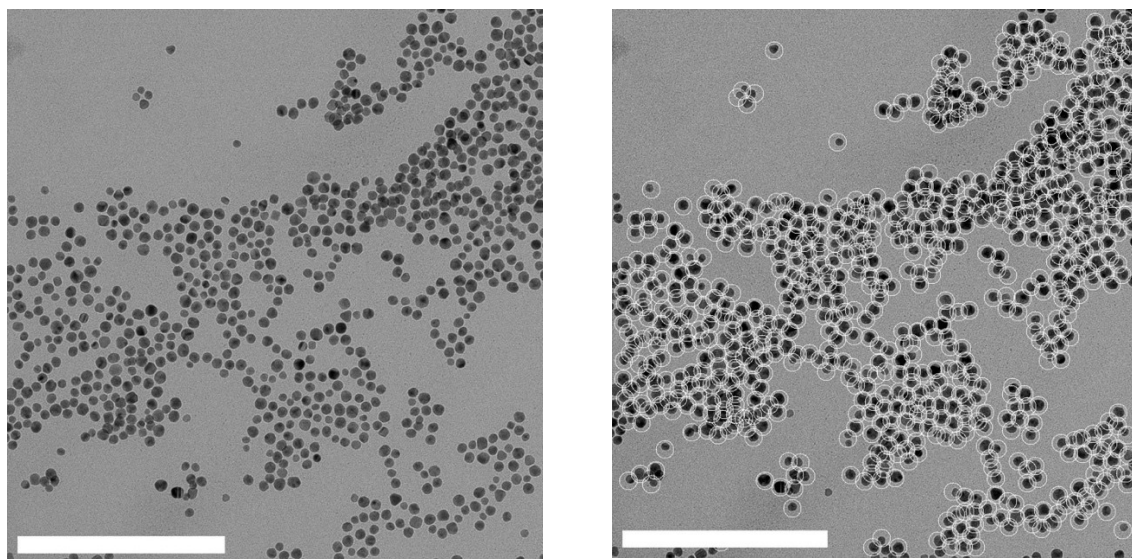


Figure S 36 - Left; raw micrograph of gold nanoparticles. Right; particles selected via automated picking. Scale bar 200 nm.

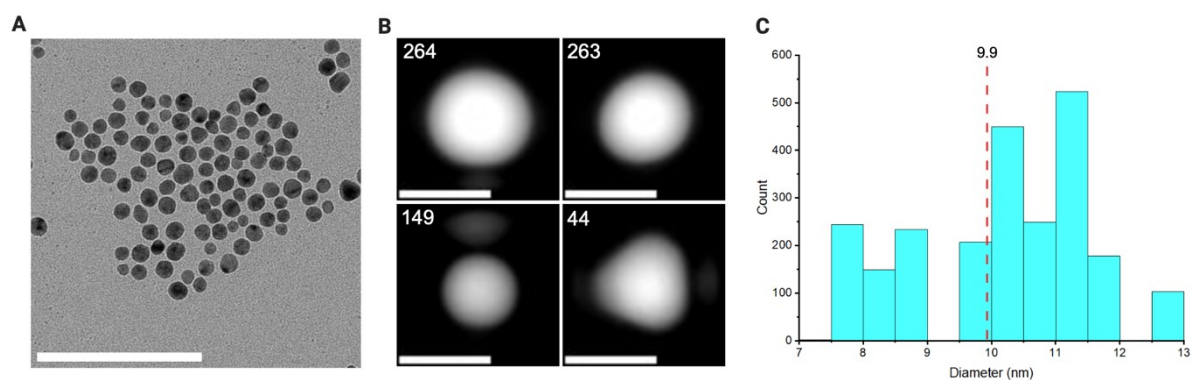


Figure S 37 – Au10 system A) raw example micrograph, scale bar 100 nm B) Example 2D classes including the class population numbers, scale bar 10 nm C) histogram of class average sizes with binning of 0.5 nm.

Additional Thresholding tests of Au10

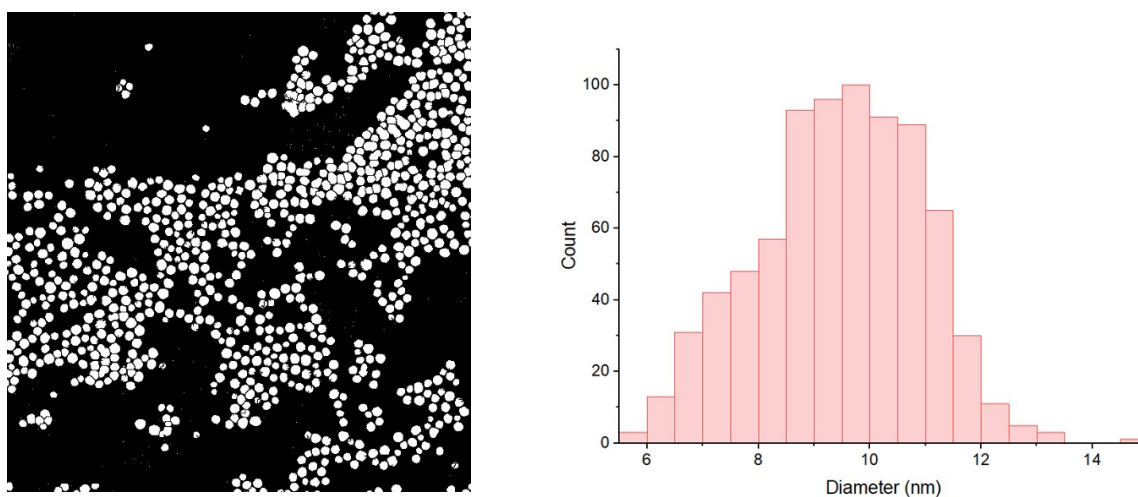


Figure S 38 – Left; threshold of gold nanoparticles in Fiji. Right; Histogram of thresholding result of the diameter

8 CryoSPARC Workflow

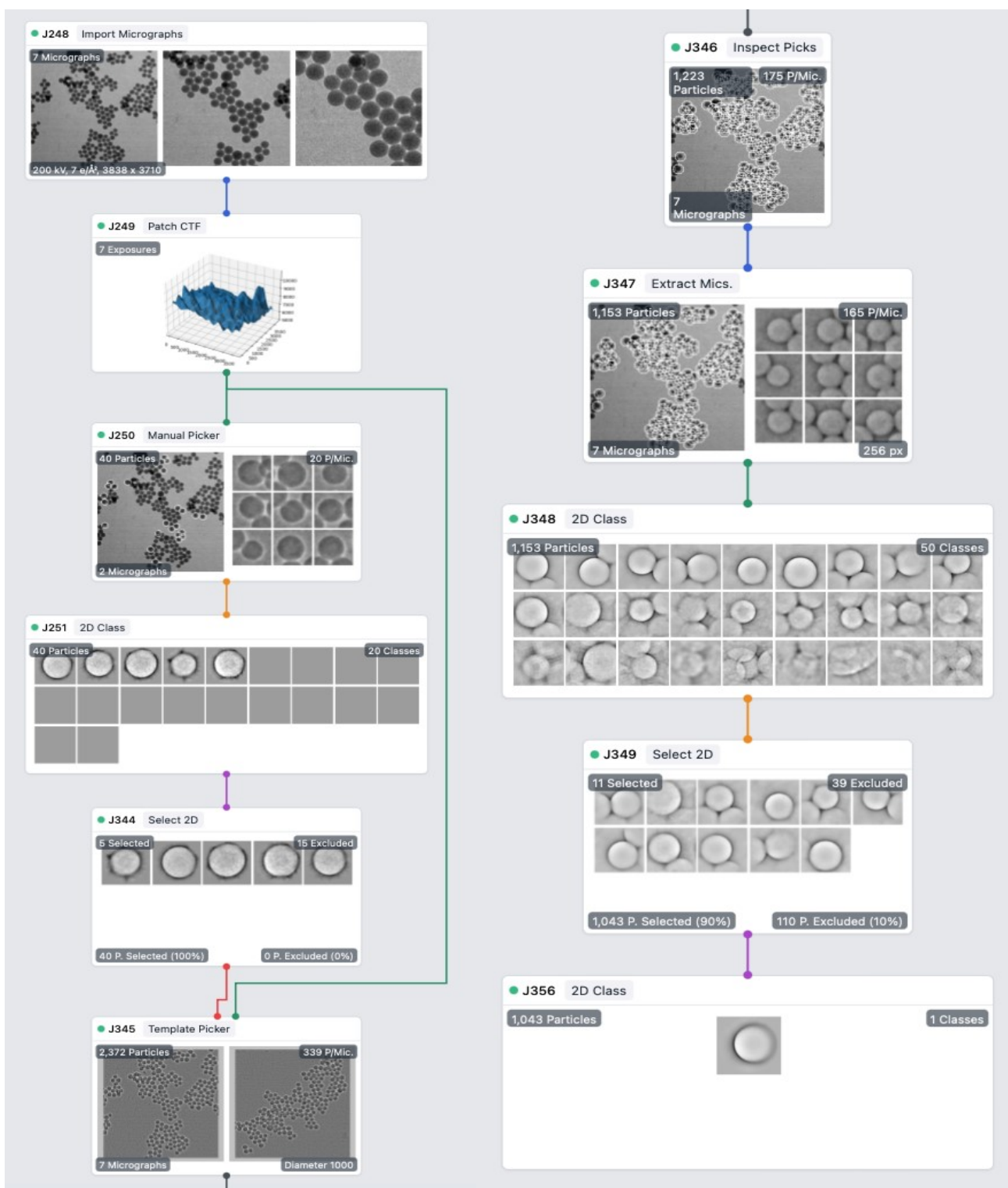


Figure S 39 - Screenshot of the workflow of cryoSPARC software for PS10 from importing to varying collections of 2D classes, including a final single class average.

9 References

- 1 S. Jiang, M. Mottola, S. Han, R. Thiramanas, R. Graf, I. Lieberwirth, V. Mailänder, D. Crespy and K. Landfester, *Particle & Particle Systems Characterisation*, 2020, **37**, 1900484.
- 2 S. Jiang, K. Landfester and D. Crespy, *RSC Adv*, 2016, **6**, 104330–104337.
- 3 T. P. Doan-Nguyen, S. Jiang, K. Koynov, K. Landfester and D. Crespy, *Angewandte Chemie International Edition*, 2021, **60**, 18094–18102.